J. Fluid Mech. (1975), *vol.* 67, *part* 4, *pp.* 647–655
Printed in Great Britain

The expansion of a hypersonic turbulent boundary layer at a sharp corner

By A. W. BLOY

Department of the Mechanics of Fluids, University of Manchester, England

(Received 26 April 1974)

A sharp wedge expansion flap was tested in the von Kármán Institute Longshot tunnel at Mach 16 and data on the wall pressure and heat transfer were obtained. Pitot pressure measurements in the boundary layer just ahead of the expansion flap were also made. The surface data are compared with predictions from a characteristics solution for the boundary-layer expansion and from a simple heat-transfer theory.

1. Introduction

In the area of turbulent viscous–inviscid interactions, the expansion of a hypersonic turbulent boundary layer at a sharp corner is a problem which has received little attention. Previous experimental studies have been restricted to Mach 5 and below and the main aim of the present study was to obtain surface data for a sharp wedge expansion corner in a Mach 16 flow. Zakkay, Toba & Kuo (1964) and Otis (see Reeves 1973) observed relaminarization of the expanding turbulent boundary layer, while Delery & Masure (1968) demonstrated the inviscid nature of the boundary-layer expansion. They applied the method of rotational characteristics to the expansion of the supersonic part of the initial boundary layer and found good agreement between the theoretical and experimental Pitot and static pressure profiles. The prediction of the present flows would provide a severe test for any theoretical method since the expanded boundary layer in the corner region is far from equilibrium.

2. Apparatus

The measurements were made in the von Kármán Institute Longshot tunnel using nitrogen as the test gas. The Longshot tunnel is a form of gun tunnel using a heavy piston (weighing from 2 to 7 kg) to produce a compression overshoot. The high-temperature high-pressure gas produced in the compression cycle is then trapped in a reservoir by the closing of a system of small valves as the piston rebounds. The test conditions decay monotonically during 10–20 ms of running time as the gas trapped in the reservoir exhausts through the 6° half-angle, conical nozzle into the test section. A fuller description of the tunnel has been given by Richards & Enkenhus (1970). The present tests were made at a nominal Mach number of 16 and all the data were taken 2 ms after the peak flow conditions.

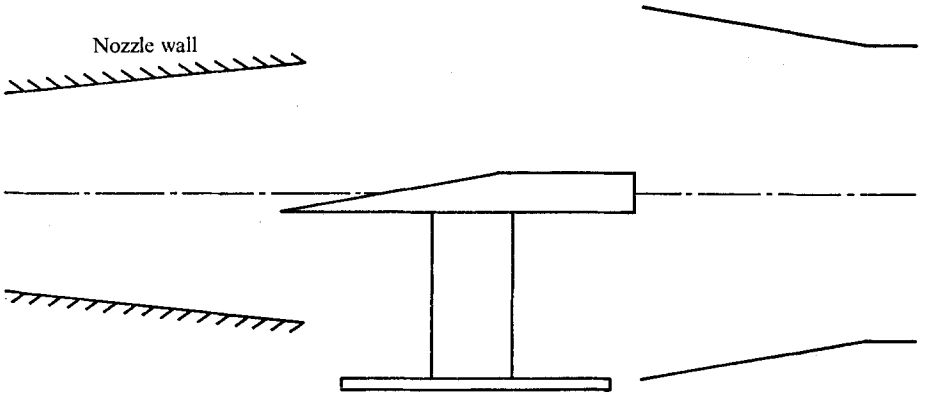

FIGURE 1. Diagram of the model in the Longshot tunnel.

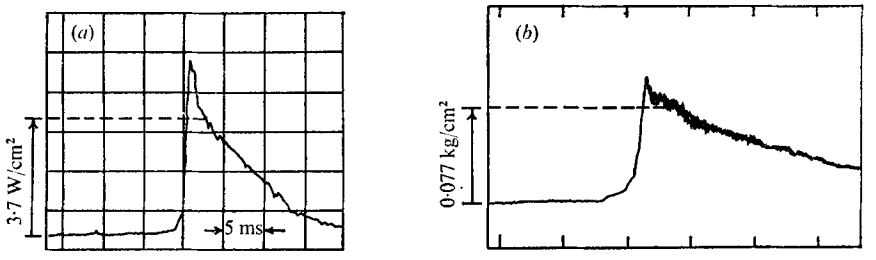

FIGURE 2. Typical traces; $M_\infty = 16$, $Re_\infty = 2.9 \times 10^5\,\mathrm{cm}^{-1}$, $H_w/H_\infty = 0{\cdot}13$.
(*a*) Turbulent heat transfer. (*b*) Wall pressure.

The relevant conditions in the reservoir were $p_0 = 3260$ atm and $T_0 = 1700\,^\circ\mathrm{K}$, although owing to real-gas effects the equivalent supply conditions of the perfect gas flow in the test section were $p_0 = 4930$ atm and $T_0 = 2160\,^\circ\mathrm{K}$. The nominal free-stream unit Reynolds number was $2{\cdot}9 \times 10^5\,\mathrm{cm}^{-1}$.

The model was a sharp flat plate inclined at an angle of incidence of 10·6° and fitted with an adjustable trailing-edge flap. The flat plate was 30 cm long and the flap 18 cm long, while the model span was 18 cm. The leading-edge thickness was about 0·005 cm and tests were made at flap angles of 0, $-5°$, $-10°$ and $-15°$. Figure 1 illustrates the model in the Longshot tunnel. The model was instrumented with thin-film, platinum-on-glass, resistance thermometers and static pressure orifices in the region of the centre-line. The surface temperature signals from the thin-film gauges were converted into the heat-transfer rate by analog networks. Pressures were measured using Hidyne variable-reluctance differential pressure transducers fitted with 0·1, 0·25, 0·5 and 3·0 psi diaphragms and connected by tubing to 3 mm diameter orifices. Typical wall pressure and heat-transfer-rate traces are shown in figure 2.

A problem associated with the use of thin-film gauges in the Longshot tunnel is abrasion of the gauges by high-speed particles. The resistances of the thin-film gauges were checked before and after a run and average increases of 5 % for the gauges on the wedge and 2 % for the gauges on the 5° expansion flap were

found. It appeared, however, that the flow abrasion did not affect the heat-transfer measurements in the period of interest.

For the Pitot pressure profile, four individual probes spaced across the centre-span were used and the pressures were measured using Kistler type 601 A, 0–250 atm and 603 B, 0–200 atm piezoelectric transducers.

3. Results and discussion

Pitot pressure measurements were made in the boundary layer on the wedge 0·5 cm ahead of the corner position with the flap set at 0°. The data were used to determine the Mach-number profile shown in figure 3(*a*), where the static pressure was assumed constant across the boundary layer and was taken to be the estimated inviscid pressure with an allowance for the turbulent boundary-layer displacement. This pressure agrees with the wall pressure measurements described later. The boundary-layer thickness δ was estimated from the profile data and the schlieren photographs, while the subscript e, in the figure, refers to the conditions at the edge of the boundary layer. In order to estimate the velocity and enthalpy profiles, the linear Crocco enthalpy–velocity relation with a unit Prandtl number was used. This relation, which is usually representative of 'flat-plate' boundary layers (see Bushnell *et al.* 1969), gives

$$(H-H_w)/(H_e-H_w) = U/U_e, \tag{1}$$

where the subscript w refers to the conditions at the wall. H and H_e were eliminated from the Crocco relationship by using the energy equation

$$H = C_p T + \tfrac{1}{2}U^2 = \frac{C_p}{\gamma R}a^2 + \tfrac{1}{2}U^2 = \frac{U^2}{(\gamma-1)M^2} + \tfrac{1}{2}U^2; \tag{2}$$

this resulted in a quadratic equation solvable for U/U_e. The solution was then substituted into (1) to find H/H_e. The velocity profile is shown in figure 3(*b*) and it can be seen that the outer profile data lie approximately on the curve given by the power law with $N = 9$, i.e.

$$U/U_e = (y/\delta)^{\frac{1}{9}}, \tag{3}$$

which implies that the turbulent boundary layer is not fully developed. This agrees with the results of previous studies, e.g. Hopkins *et al.* (1972), which have indicated that the boundary layer may not be fully developed in the region just after transition and in which values of N between 6 and 12 have been found. Total-temperature measurements in the boundary layer were made by a technique using fine tungsten wires, although the conditions in the Longshot tunnel made the accurate assessment of corrections very difficult. The measurements were therefore discarded and so did not allow a check on the validity of the Crocco relation.

From the schlieren photographs, shown in figure 4 (plate 1), the beginning of transition in the region 12 cm from the leading edge can be seen. The weak expansion waves emanating from the boundary layer at $x = 7{\cdot}5$ cm are due to a misalignment in incidence of 0·2° between the leading-edge section and the plate. At the corner, the boundary layer is 4·6 mm thick and it appears that there is very

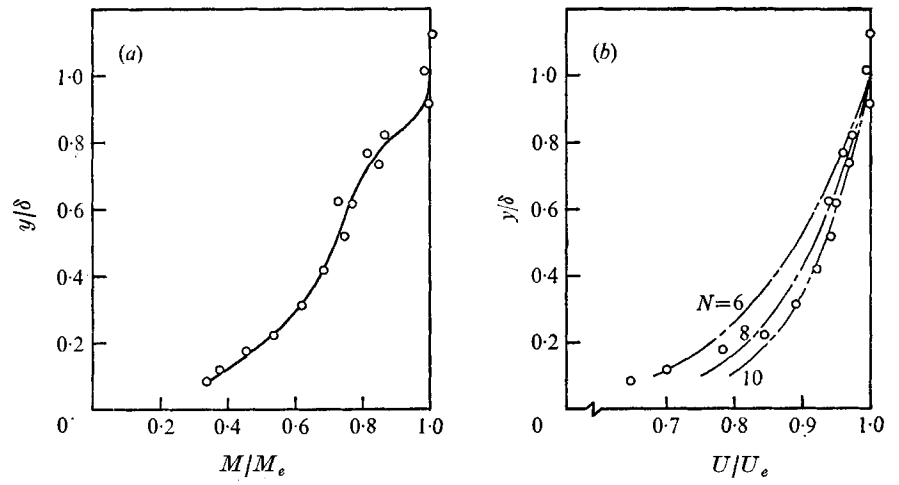

FIGURE 3. Turbulent boundary-layer profile data at $x = 29{\cdot}5$ cm; $M_e = 7{\cdot}35$, $\delta = 4{\cdot}6$ mm, $H_w/H_e = 0{\cdot}13$, $Re_\theta = 3300$. (*a*) ○, Mach-number data. (*b*) ○, velocity data; ———, velocity power laws with $N = 6$, 8 and 10.

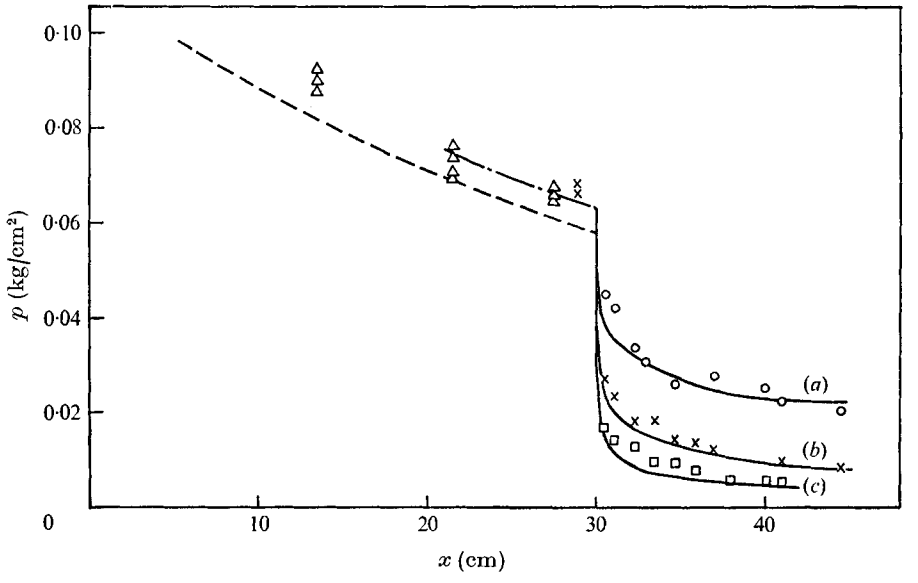

FIGURE 5. Pressure distribution on the expansion-corner model; $M_\infty = 16$, $Re_\infty = 2{\cdot}9 \times 10^5$ cm^{-1}, $H_w/H_\infty = 0{\cdot}13$. ———, estimated inviscid pressure distribution; ———, estimated pressure distribution including turbulent boundary-layer displacement; △, present experimental data, flap angle $\alpha = 0°$; ——, method of characteristics. (*a*) $\alpha = -5°$; ○, present experimental data. (*b*) $\alpha = -10°$; ×, present experimental data. (*c*) $\alpha = -15°$; □, present experimental data.

little upstream influence, while downstream of the corner, the edge of the boundary layer (figures 4(*a*) and (*b*) only) and a sublayer (figure 4(*b*) only) can be seen.

The experimental pressure data for the expansion corners are shown in figure 5. On the wedge, the data are in good agreement with the estimated pressure dis-

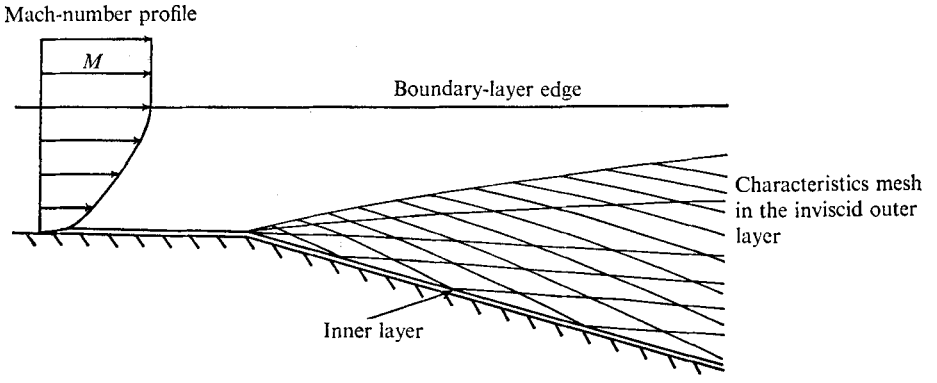

FIGURE 6. Two-layer model of turbulent boundary-layer expansion.

tribution which includes the turbulent boundary-layer displacement. To allow for the conicity of the free-stream flow, the pressure on the wedge was calculated using the local angle of attack and local flow conditions, while the growth of the turbulent boundary-layer displacement δ^* was estimated using δ^*/δ, calculated from the profile data, and $d\delta/dx$, measured from a schlieren photograph. The data downstream of the corner are compared with the results from the characteristics solution for the boundary-layer expansion. The initial Mach-number and velocity profiles for the solutions are those given in figures 3(*a*) and (*b*). A diagram of the interaction model is shown in figure 6. It is assumed that there is no upstream influence and the boundary layer is divided into an inviscid supersonic outer layer and an inner layer. The division between the two layers is taken as the streamline which originates from the sonic point in the initial flow. The outer layer is then analysed by the method of rotational characteristics while the inner layer is assumed to have no effect on the interaction and so remains unchanged. Note that the thickness of the inner layer is only about 4 % of the boundary-layer thickness. The numerical solution for the outer layer proceeds downstream of the first Mach line with the total expansion angle divided into a series of steps and makes use of the fact that, at the corner, the flow is locally a Prandtl–Meyer expansion. Typically, forty points across the boundary layer and twenty steps at the corner are taken, while the finite-difference equations used are those given by Oosthuizen (1967). The agreement between the theory and experiment is favourable for all three expansion angles. In the theoretical solution, allowance was made for the non-parallel flow in the boundary layer upstream of the corner, while the flow in the boundary layer was assumed to be two-dimensional.

The heat-transfer data are shown in figure 7, together with theoretical estimates. On the wedge, the heat transfer is typical of transition at high Mach number. A region of laminar flow is followed by an almost equal length of transitional flow to the point of peak heating. The theoretical estimates were obtained by assuming local flat-plate boundary-layer similarity of the laminar and turbulent flows. Thus the main effect of the pressure gradient was assumed to be on the thickness and not on the shape of the boundary-layer profiles. Lees (1956) has

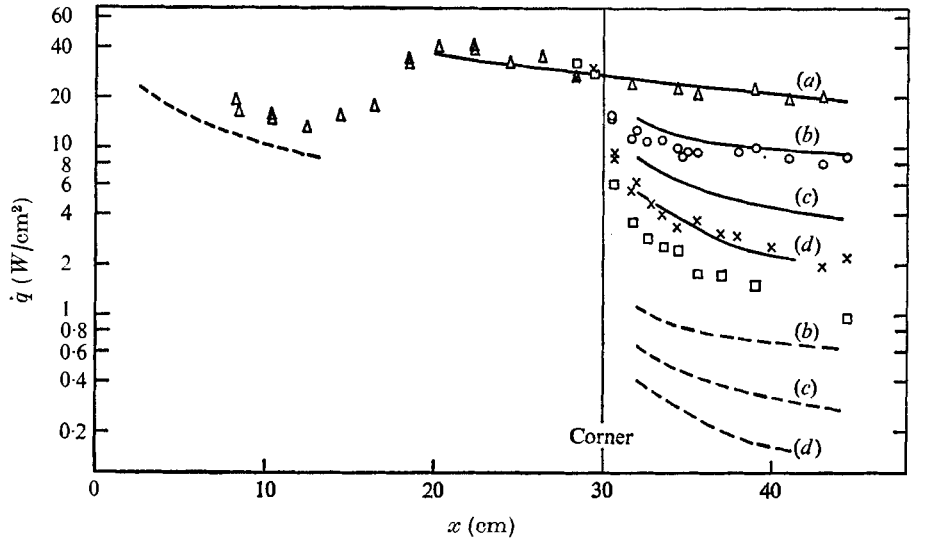

FIGURE 7. Heat-transfer-rate distribution on the expansion-corner model; $M_\infty = 16$, $Re_\infty = 2{\cdot}9 \times 10^5\,\mathrm{cm}^{-1}$, $H_w/H_\infty = 0{\cdot}13$. ---, laminar boundary-layer theory; ——, turbulent boundary-layer theory. (*a*) $\alpha = 0°$; △, present experimental data. (*b*) $\alpha = -5°$; ○, present experimental data. (*c*) $\alpha = -10°$; ×, present experimental data. (*d*) $\alpha = -15°$; □, present experimental data.

described the laminar theory. The turbulent theory uses the energy thickness Γ defined by

$$\Gamma = \int_0^\delta \frac{\rho\mu}{\rho_e u_e}\left(1-\frac{H}{H_e}\right)dy, \tag{4}$$

so that the integral form of the energy equation may be written as

$$d(\rho_e u_e H_e \Gamma)/dx = \dot{q}. \tag{5}$$

Thus Γ can be found directly from the measured heat-transfer-rate distribution $\dot{q}(x)$ as

$$\Gamma = \frac{1}{\rho_e u_e H_e}\int_0^x \dot{q}\,dx \tag{6}$$

and the inaccuracy of defining a virtual origin is avoided. The predicted heat-transfer rate is then obtained from the local flat-plate value for the Stanton number, based on the local flow conditions (see Walker 1960). The Stanton number is derived from the flat-plate skin-friction coefficient given by

$$\tfrac{1}{2}C_f = 0{\cdot}013\,Re_\theta^{-\frac{1}{4}}(\mu^*/\mu_e)^{\frac{1}{4}}\rho^*/\rho_e \tag{7}$$

and the relation between the energy thickness Γ *and the momentum thickness* θ, which is

$$\Gamma = F[(H_r - H_w)/H_e]\,\theta. \tag{8}$$

F is the Reynolds analogy factor, while the subscript r denotes the recovery condition and starred quantities are to be evaluated at the Eckert (1955) reference temperature

$$T^*/T_e = 0{\cdot}5\,(T_w/T_e + 1) + 0{\cdot}044r\,M_e^2, \tag{9}$$

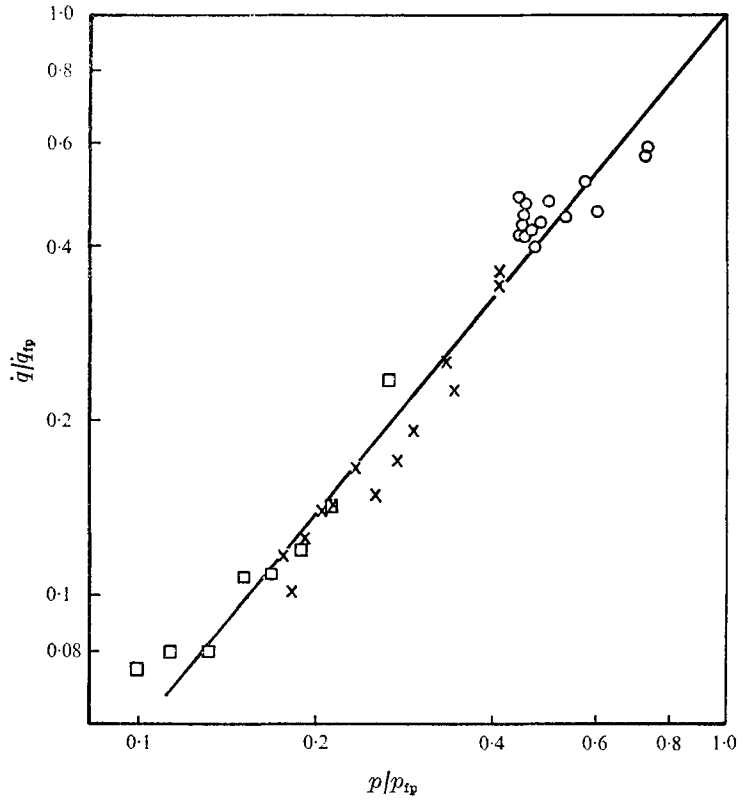

FIGURE 8. Correlation of present heat-transfer-rate data downstream of the expansion corner; $M_\infty = 16$, $Re_\infty = 2{\cdot}9 \times 10^5\,\mathrm{cm}^{-1}$, $H_w/H_\infty = 0{\cdot}13$. ○, experimental data at $\alpha = -5°$; ×, experimental data at $\alpha = -10°$; □, experimental data at $\alpha = -15°$; ——, mean line through data.

where r is the recovery factor. It can be seen from figure 7 that there is good agreement between the turbulent heat-transfer prediction and the experimental data from the wedge. The Reynolds analogy factor F and the recovery factor r were taken as 1·1 and 0·9.

It is encouraging to note here that the energy thickness of the boundary layer just upstream of the corner estimated from the measured heat-transfer distribution and using (6) is approximately $\Gamma = 0{\cdot}036\,\delta$, while from the profile data, the result is $\Gamma = 0{\cdot}032\,\delta$. Some of the difference can be accounted for by the free-stream conical flow, so that the two estimates of Γ are in good agreement.

The heat-transfer distributions downstream of the corner are similar in form to the wall pressure distributions, a feature which has also been found for compression-corner flow (see Coleman & Stollery 1972). This similarity therefore suggests that there is a direct relation between the local heat transfer and wall pressure. The present data, shown in figure 8, give the approximate correlation

$$\dot{q}/\dot{q}_{fp} = (p/p_{fp})^{1{\cdot}23}, \tag{10}$$

where the subscript fp refers to the conditions on the flat-plate model, i.e. at zero flap angle. An indication that the boundary layer downstream of the corner is

turbulent is given by the heat-transfer traces. For the decaying reservoir conditions in the Longshot tunnel, the heat transfer downstream of the corner decays at a rate similar to that for the region of turbulent flow just upstream of the corner. This rate of decay is considerably higher than that in the laminar flow region near the leading edge. Predictions from both the local flat-plate turbulent boundary-layer similarity theory and the laminar equivalent of this theory are also shown in figure 7, where the pressure in the boundary layer was taken as the measured wall pressure and the energy thickness Γ was estimated from the experimental heat-transfer-rate distributions. In the laminar theory, the only differences from the turbulent boundary-layer analysis, described earlier, are that (7) is replaced by the relation obtained from the Eckert (1955) reference-enthalpy method, i.e.

$$\tfrac{1}{2}c_f = 0{\cdot}220C^*/Re_\theta, \tag{11}$$

while the Reynolds analogy factor and the recovery factor are $Pr^{*-\frac{2}{3}}$ and $Pr^{*\frac{1}{2}}$. It can be seen from the figure that the experimental data lie closer to the predictions from the turbulent theory and are well above the laminar theoretical results. The turbulent theory predicts the data reasonably well for the 5° expansion-corner case but overpredicts by 50–75 % for the 10° and 15° expansion corners. A significant effect on the heat transfer to the wall may be the reduction of turbulent mixing associated with the streamline curvature. Thomann (1968) measured the heat-transfer distributions at Mach 2·5 on both a flat plate and a convex wall where the wall pressures were kept similar by using external compression or expansion surfaces. The results showed that the heat transfer on the convex surface was considerably lower than that on the flat plate. Thomann attributed the difference to the effect of the normal pressure gradient on the turbulent mixing in the boundary layer.

4. Conclusions

High-Mach-number data have been obtained for the expansion of a turbulent boundary layer at a sharp corner and the data have been compared with the results from two simple analyses. Predictions from a characteristics solution for the expansion of the boundary layer and external flow compare favourably with the experimental wall pressure data. When compared with results from the local flat-plate boundary-layer similarity theory, the heat-transfer-rate data downstream of the corner lie much closer to the turbulent predictions than to the laminar predictions.

The author wishes to acknowledge Dr B. E. Richards and E. Backx for their detailed comments and is grateful to the Royal Society for financial support, during the course of this work, in the form of a fellowship in the European Science Exchange Programme.

REFERENCES

BUSHNELL, D. M., JOHNSON, C. B., HARVEY, W. D. & FELLER, W. V. 1969 Comparison of prediction methods and studies of relaxation in hypersonic turbulent nozzle-wall boundary layers. *N.A.S.A. Tech. Note*, D-5433.

COLEMAN, G. T. & STOLLERY, J. L. 1972 Heat transfer from hypersonic turbulent flow at a wedge compression corner. *J. Fluid Mech.* **56**, 741–752.

DELERY, J. & MASURE, B. 1968 Action d'une variation brusque de pression sur une couche limite turbulente en écoulement supersonique. *Recueil de notes sur l'Activité de l'ONERA*, pp. 25–26.

ECKERT, E. R. G. 1955 Engineering relations for skin friction and heat transfer to surfaces in high velocity flow, *J. Aero. Sci.* **22**, 585.

HOPKINS, E. J., KEENER, E. R., POLEK, T. E. & DWYER, H. A. 1972 Hypersonic turbulent skin friction and boundary-layer profiles on non-adiabatic flat plates, *A.I.A.A. J.* **10**, 40–48.

LEES, L. 1956 Laminar heat transfer over blunt-nosed bodies at hypersonic flight speeds. *Jet Propulsion*, **26**, 259–269.

OOSTHUIZEN, P. H. 1967 An analysis of the interaction of a boundary layer and the corner expansion wave in supersonic flow. *U.T.I.A.S. Tech. Note*, no. 117.

REEVES, B. L. 1973 A two-layer model of high speed two- and three-dimensional turbulent boundary layers with pressure gradient, surface mass injection and entropy layer swallowing. *A.I.A.A. Paper*, no. 73–135.

RICHARDS, B. E. & ENKENHUS, K. R. 1970 Hypersonic testing in the VKI Longshot free-piston tunnel. *A.I.A.A. J.* **8**, 1020–1025.

THOMANN, H. 1968 Effect of streamwise wall curvature on heat transfer in a turbulent boundary layer. *J. Fluid Mech.* **33**, 283–292.

WALKER, G. K. 1960 A particular solution to the turbulent boundary layer equations. *J. Aero. Sci.* **27**, 715–716.

ZAKKAY, V., TOBA, K. & KUO, T. J. 1964 Laminar, transitional and turbulent heat transfer after a sharp corner, *A.I.A.A. J.* **2**, 1389–1395.

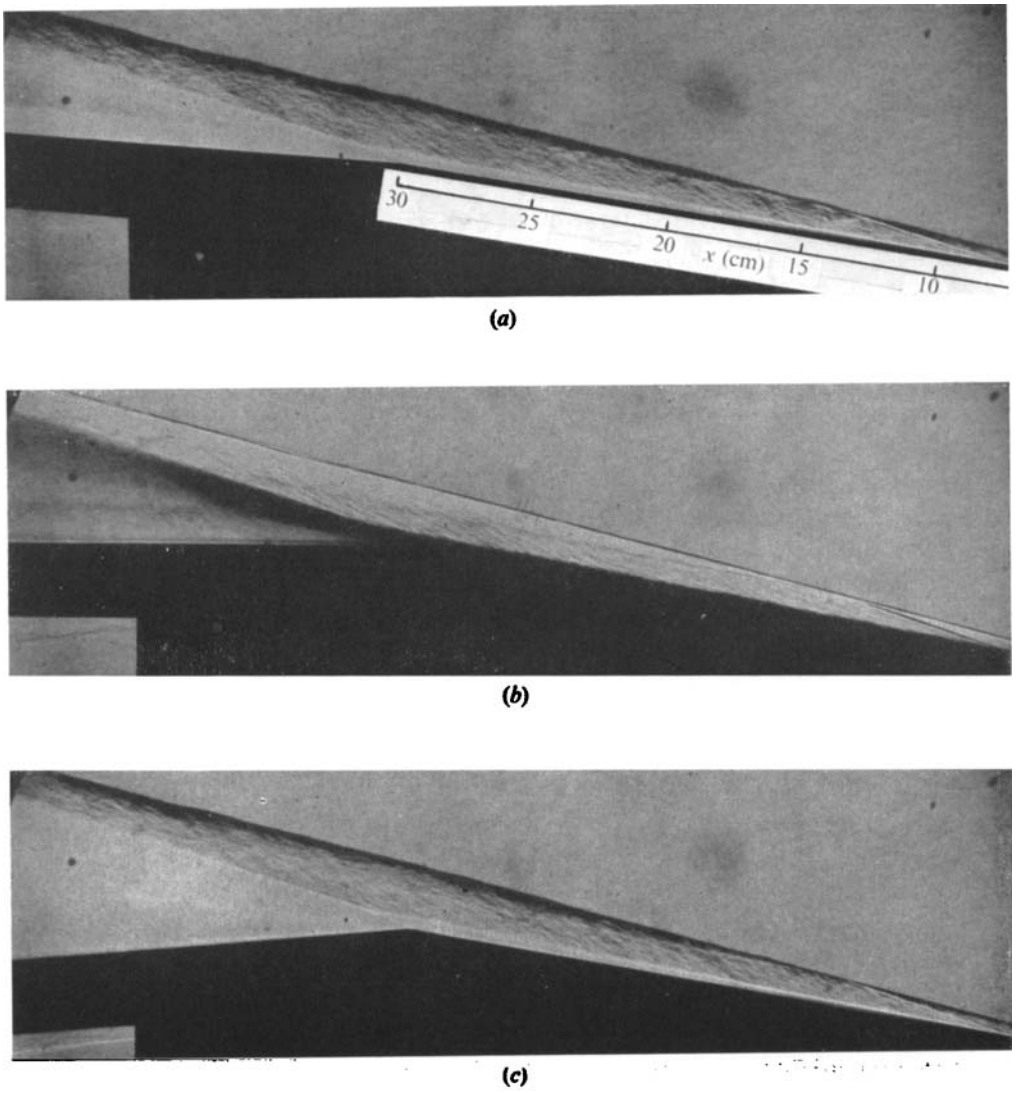

FIGURE 4. Schlieren photographs of the flow over (*a*) the 5° expansion corner, (*b*) the 10° expansion corner and (*c*) the 15° expansion corner; $M_\infty = 16$, $Re_\infty = 2{\cdot}9 \times 10^5\,\mathrm{cm}^{-1}$, $H_w/H_\infty = 0{\cdot}13$.